IEEE Access
Multidisciplinary | Rapid Review | Open Access Journal

Received January 10, 2022, accepted January 16, 2022, date of publication January 25, 2022, date of current version January 31, 2022.

Digital Object Identifier 10.1109/ACCESS.2022.3145978

Topographic SLAM Using a Single Terrain Altimeter in GNSS-Restricted Environment

JUNWOO JANG AND JINWHAN KIM, (Member, IEEE)
Department of Mechanical Engineering, Korea Advanced Insititute of Science and Technology, Daejeon 34141, South Korea

Corresponding author: Jinwhan Kim (jinwhan@kaist.ac.kr)

This work was supported by the National Research and Development Program through the National Research Foundation of Korea (NRF) funded by the Ministry of Science and ICT (MSIT) under Grant 2020M3C1C1A02086303.

ABSTRACT In a Global Navigation Satellite System (GNSS)-restricted area, a mobile robot navigation system exploits surrounding environment information. For an aerial or underwater vehicle, undulating terrain of a land or seabed surface is a valuable information resource that leads to the development of terrain-referenced navigation (TRN) algorithms. However, due to the vast amount of a vehicle's activity area, surveying all the regions to obtain a high-resolution terrain map is impractical and requires simultaneous localization and mapping (SLAM) as a highly desirable capability. This paper presents a topographic SLAM algorithm using only a single terrain altimeter, which is low-cost, computationally efficient, and sufficiently stable for long-term operation. The proposed rectangular panel map structure and update method enable robust and efficient SLAM. As terrain elevation changes are inherently nonlinear, an extended Kalman filter (EKF)-based SLAM filter is adopted. The feasibility and validity of the proposed algorithm are demonstrated through simulations using terrain elevation data from a real-world undersea environment.

INDEX TERMS Terrain-referenced navigation, simultaneous localization and mapping, extended Kalman filter, topography, bathymetry, autonomous underwater vehicle.

I. INTRODUCTION

Localization is one of the most critical capabilities for autonomous robotic vehicles. These vehicles are generally equipped with proprioceptive motion sensors for dead-reckoning using onboard motion sensors with no position fixes that are susceptible to integration drift error, which grows in time without bound and can significantly degrade navigation accuracy. Therefore, the Global Navigation Satellite System (GNSS), which provides absolute position fixes, has been widely used for vehicle navigation and localization in open outdoor environments.

However, GNSS signals are not always available or reliable. The GNSS is unreliable to underwater vehicles operating under the water surface because electromagnetic waves that carry GNSS signals cannot penetrate more than several centimeters of water. The GNSS may not be available even for flying vehicles in some GNSS-restricted areas such as forests or urban canyons and for space exploration on other planets. Moreover, the GNSS may become unavailable in hostile scenarios because radio signals are vulnerable to electromagnetic jamming and spoofing.

Terrain-referenced navigation (TRN) can be an appropriate substitute for a GNSS in GNSS-restricted environments. It was used before the development of the GNSS in aerial navigation and was most widely adopted among geophysical navigation systems. There are several approaches to exploiting terrain information, such as using a terrain profile for matching with obtained measurements or using terrain elevation changes from moment to moment. However, the TRN is map-based navigation, which requires surveying all the vehicle's activity area in advance—crucially daunting for extreme environments such as underwater.

Hence, simultaneous localization and mapping (SLAM) is highly desirable for navigating previously unexplored environments. Although SLAM may not completely remove position errors, it can bound the vehicle's position error relative to the generated map, and thus any point in the map can be revisited under some position errors. Among the vast body of literature, relatively few papers deal with topographic SLAM; most use multibeam sensors to obtain a terrain profile. Although it is a reasonable approach because SLAM is a demanding technique that typically takes

The associate editor coordinating the review of this manuscript and approving it for publication was Mauro Gaggero.

highly informative measurements (e.g., camera or Lidar), developing a computationally efficient system with a minimal sensor suite is required for a small mobile vehicle. This demand emphasizes underwater systems, where a multibeam echosounder (MBE) is highly cumbersome and expensive.

This paper presents a topographic SLAM algorithm using a only single altimeter. The rectangular panel map structure using bilinear interpolation represents undulating terrain and enables single measurement SLAM by reducing the estimating map state relative to observation. The gradient of panel map and altimeter measurement can determine the vehicle's position if the vehicle is located at a specific panel. If the vehicle does not belong to a particular panel, it is possible to update stochastically using weighted grid partitioning (WGP). An extended Kalman filter (EKF) simplifies the problem and maintains a manageable computational burden. This paper also demonstrates that the proposed algorithm can bound the computational complexity regardless of the map size. Various simulations using real-world undersea terrain data were performed, validating that the proposed algorithm sufficiently bounds the position error and generates an approximated terrain map, even with minimal sensor equipment.

The rest of the paper is organized as follows. Section II outlines existing research and related work. Section III presents an overview of the proposed algorithm, and the algorithm's formulation is described in Section IV. In Section V, simulation results based on the proposed topographic SLAM algorithm are presented and discussed. Finally, the conclusions from this research are drawn in Section VI.

II. RELATED WORK

Terrain-referenced (also known as terrain-relative or terrain-aided) navigation was first introduced in the 1970s, and the seminal terrain contour matching (TERCOM) algorithm was successfully applied to cruise missile navigation even before the GNSS was fully operational [1]. The operational TERCOM algorithm used a mean absolute difference algorithm for computational efficiency and moderate storage requirements. Since then, several algorithms have been developed for terrain-relative navigation. Sandia Inertial Terrain Aided Navigation (SITAN) is one of the early terrain-referenced techniques incorporating the Kalman filter algorithm [2]. Terrain profile matching (TERPROM), which was initially developed for cruise missiles, is now used for military jets [3].

Even in the current GNSS era, terrain-based techniques are still regarded as necessary and valuable because a GNSS may not always be available and reliable, due primarily to its vulnerability to electric warfare techniques such as jamming and spoofing. Its capability for planetary landing to explore other planets and moons has also been investigated [4].

Although not as established as in aerospace applications, there has been some research on TRN using bathymetric information in marine applications for underwater vehicles [5]–[9]. A survey paper by Carreno *et al.* [10] compared several mathematical filter models for TRN techniques for autonomous underwater vehicles (AUVs) with a description of the original TERCOM algorithm. The paper discussed map-based navigation techniques for AUVs that assume the availability of an undersea terrain map.

SLAM enables building a map and simultaneously localizing the observer with respect to the map. It has been one of the more highly focused research areas in vehicle navigation and robotics since its advent in the late 1980s and early 1990s [11], [12]. Extensive literature exists on various SLAM approaches. Several SLAM algorithms using discrete landmarks as map features were developed based on Kalman and information filters [13]. Research for applying SLAM to aerial vehicles has also been performed [14], [15]. As a particle filtering approach, a hybrid structure based on Rao-Blackwellization—combining an analytical filter and a particle filter (e.g., FastSLAM)—was developed and has been applied to various applications [13]. However, these techniques assume that the environment can be represented by a map of distinguishable landmark features, which may not be justifiable in some natural environments.

The TRN approach can be extended to SLAM applications in environments with few to no salient features and only terrain elevation. This extension is valuable in underwater vehicle applications because a GNSS is inherently unavailable under the water surface. Only a few papers describe undersea bathymetric SLAM, most of which discuss the reconstruction of subsea terrain maps through offline computations using a substantial set of measurements from a high-performance bathymetric sensor like an MBE [16]–[19]. Reference [16] discussed TRN in an unknown environment based on the parametric representation of a subsea terrain using a pre-trained neural network model and compared the performance between the EKF and the unscented Kalman filter (UKF). A large-scale terrain map combining several small sub-maps obtained by multibeam sonar measurements was created using a delayed Kalman filter in [17].

Barky *et al.* proposed a bathymetric SLAM algorithm using a Rao-Blackwellized particle filter and new grid-based map representation incorporating multibeam echosounder measurements that can be implemented with less computational cost and data storage while maintaining the accuracy from previous studies [20], [21]. Another approach has been conducted that matches the bathymetric profiles to increase association accuracy by reducing computation [22]. More recently, Teng *et al.* conducted bathymetric SLAM based on a graph structure to achieve robustness in preventing invalid loop-closures [23]. Some research has been proposed to reduce computation and data storage dramatically by using only a featured area [24] or exploiting the sparce depth measurements obtained from a Doppler Velocity Log (DVL) [25].

However, to the best of our knowledge, existing studies have not addressed the algorithms that can be applied to topographic/bathymetric SLAM using a low-cost single terrain altimeter. This study assumes that a minimal set of sensors, including basic motion sensors and an altimeter,

are available. This assumption requires a suitable terrain map representation scheme, discussed in Section IV.

III. TOPOGRAPHIC SLAM

Topography is the study of mapping terrain surfaces, including generating surface elevation data. Aerial or satellite imagery can be used to cover a large area efficiently. Furthermore, various types of range sensors, such as laser, radar, and sonar, can directly measure the distance between the vehicle and the terrain surface. Bathymetry is underwater topography—the study of mapping underwater terrain using a hydrographic survey measuring the depth of a body of water (e.g., an ocean). Bathymetric information is essential for ocean space utilization, such as ship navigation and exploration and the development of ocean environments. Typically, a bathymetric survey is performed using a research vessel equipped with an MBE. The MBE is a sophisticated bathymetric sensor that uses a swath of soundings for high-resolution mapping. A bathymetric survey using an MBE generally requires post-processing to create a subsea terrain map.

A crucial requirement for terrain-relative navigation is the availability of a reference map or a terrain elevation model. If a map is available or given in advance, map-based navigation can be performed. Since the advent of the terrain-referenced techniques in the 1970s, terrain elevation maps such as Digital Terrain Elevation Data have been produced over vast areas on the Earth's surface using aerial photographs and satellite imageries. In contrast, most of the ocean floor has not yet been explored, primarily due to sensing difficulties—the availability of a high-precision subsea elevation map cannot be assumed in general.

The SLAM approach is necessary and can be effective when neither a map nor absolute position fixes are provided from external beacon systems (e.g., GNSS and acoustic baseline systems). Therefore, although the topographic SLAM approach applies to navigation applications for all types of vehicles, it may be more practical for underwater vehicle applications because no GNSS is available underwater and a subsea terrain map (i.e., bathymetric map) of the given area often does not exist.

Recently, the use of AUVs has become more widespread, and their feasibility and utility have already been well established. Underwater localization is a crucial capability for the reliable operation of AUVs. Onboard inertial sensors produce drift errors in the vehicle's position. Unfortunately, the GNSS, which provides an ideal sensor fusion for removing the drift errors, is not available under the water surface. As an alternative, an underwater beacon system such as long baseline (LBL) may be used for providing drift-free position fixes. However, its coverage is limited and its operation requires the pre-deployment of the beacons (or transponders) followed by a complex and time-consuming calibration process. This necessitates an algorithm that can build a map and determine the vehicle's position relative to the map simultaneously (namely the SLAM algorithm).

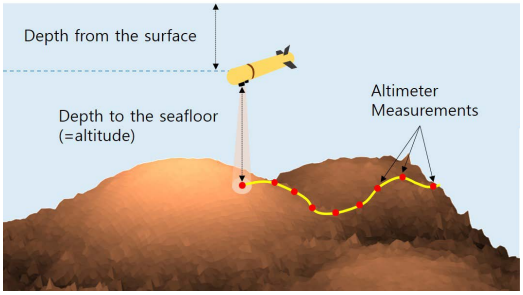

FIGURE 1. An illustration of bathymetric SLAM using an AUV with an acoustic altimeter.

Figure 1 illustrates the idea of the bathymetric SLAM algorithm proposed in this study. This study focuses on developing a computationally efficient algorithm assuming that a compact, low-cost single-beam altimeter (i.e., acoustic depth finder) is used as a bathymetric sensor instead of a relatively bulky and expensive MBE system.

Initially, the subsea terrain profile is assumed to be unknown or very coarsely defined based on sparse soundings. The proposed bathymetric SLAM approach enables generating a bathymetric map using a series of depth measurements from a single-beam terrain altimeter while estimating the vehicle's position along with onboard motion sensors simultaneously. This position estimate is calculated by combining both motion measurements provided by onboard motion sensors and position fixes obtained from the map that is being built.

At the beginning of the SLAM operation, when the bathymetric map is highly uncertain, the position estimate relies primarily on the initial pose settings and onboard sensor measurements. However, as the map uncertainty level decreases, the vehicle's position estimate can be corrected more effectively and directly using the residual error between the actual altitude measurement and the estimated altitude by the map. This approach is detailed in the next section.

IV. PROBLEM FORMULATION

A mathematical description of the proposed algorithm is described in this section. The system dynamics and measurement equations are presented, and a terrain-map-represented scheme based on rectangular tessellation is described. Accordingly, the topographic SLAM problem is formulated as a recursive estimation problem.

A. VEHICLE DYNAMICS AND MEASUREMENT EQUATIONS

The state vector to represent the vehicle's six degrees-of-freedom motion in state space can be expressed as

$$\mathbf{x}_m = \begin{bmatrix} x & y & z & \phi & \theta & \psi & u & v & w \end{bmatrix}^\top \quad (1)$$

where x, y, and z are the positions of the vehicle in global coordinates. ϕ, θ, and ψ are the vehicle's orientations in Euler angles. u, v, and w are the vehicle's velocities in the body-fixed frame. The motion of the vehicle can be computed by integrating the system dynamics model depicted in (2) over

time.

$$\dot{\mathbf{x}}_m = \mathbf{f}_m(\mathbf{x}_m, \boldsymbol{u}, \mathbf{w}) \tag{2}$$

$\mathbf{f}_m(\cdot)$ represents the nonlinear motion model. $\mathbf{u}$ is the control input vector, and $\mathbf{w}$ is the process noise due to environmental disturbances. The motion model is often expressed as kinematic equations driven by inertial sensor measurements as the control input $\mathbf{u}$, consisting of three accelerations and three angular rates.

In this problem formulation, no explicit position information is assumed to be provided to the SLAM filter as in the scenario where there are no GNSS signal available. The measurement equation is defined by Eq. (3).

$$\mathbf{z} = \mathbf{h}(\mathbf{x}_m, \eta, \mathbf{v}) \tag{3}$$

The measurement vector $\mathbf{z}$ is composed of the distance measurement to the terrain surface by an altimeter and the motion measurements provided by onboard non-inertial sensors. $\mathbf{h}(\cdot)$ is the measurement function, $\mathbf{v}$ is the measurement noise vector, and η is the surface elevation measurement of the terrain at the vehicle's current position. η is a function of the x and y position, and this functional dependency introduces severe nonlinearity in the measurement model.

The surface elevation measurement also depends on the vehicle's vertical position. Thus, the surface elevation profile in the global frame must be determined using the vertical distance to the terrain surface from the vehicle and the absolute altitude of the vehicle with respect to a specific reference surface (e.g., mean sea level). The vertical distance measurements can be obtained using exteroceptive sensors such as radar or Lidar or using acoustic altimeters. Furthermore, the vehicle's absolute (pressure) altitude relative to the reference surface is measured by proprioceptive sensors, such as barometers or pressure sensors measuring the static pressure of the ambient fluid (e.g., air or water).

B. PANEL-BASED MAP STRUCTURE

A high-resolution original terrain map is not always beneficial to navigation systems based on estimation filters. Because terrain elevation is highly nonlinear, incorporating the detailed map directly to a nonlinear estimation filter such as EKF may induce filter divergence. Robust nonlinear estimation filters, such as particle filters or point-mass filters, can fully extract the highly informative original data, but these are computationally too expensive for online applications. In [26], local terrain map is fitted to a smooth function, and TRN is operated based on a fitted function, enhancing filter convergence and accuracy. Similarly, approximating a terrain map can be advantageous to topographic SLAM.

The rectangular panel, which has elevations of four corner points, can determine the elevation of any point in the panel by bilinear interpolation as follows:

$$h_{est}(x, y) = \frac{[x_2 - x \; x - x_1]}{\Delta x \Delta y} \begin{bmatrix} h_{n1} & h_{n2} \\ h_{n3} & h_{n4} \end{bmatrix} \begin{bmatrix} y_2 - y \\ y - y_1 \end{bmatrix}. \tag{4}$$

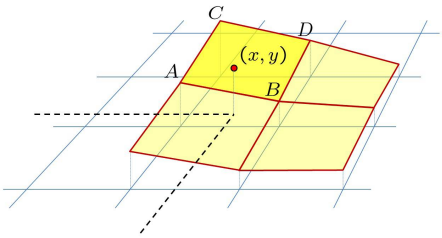

FIGURE 2. Terrain surface representation using rectangular panels.

It is assumed that the terrain surface is fairly smooth and varies continuously, and the panel size should be chosen to satisfy this assumption. All the panels are stitched and share corner points with neighboring panels, as depicted in Fig. 2. After combining all corner points defined as nodal points, the elevations at all nodal points are expressed in a vector form as

$$\boldsymbol{\eta} = \begin{bmatrix} \eta_1 & \eta_2 & \cdots \end{bmatrix}^\top. \tag{5}$$

The number of nodal points increases with the vehicle's operating region, and newly generated elevation elements are initially set to be an arbitrary value or an approximate surface elevation value if available (e.g., average altitude or depth relative to the mean sea level of the area of interest).

C. SLAM FILTER IMPLEMENTATION

The unknown elevation vector in Eq. (5), consisting of parameter states to be estimated, is introduced into the filter dynamics, augmenting the vehicle's state vector in Eq. (2). The augmented state vector is represented as

$$\begin{aligned} \mathbf{x} &= \begin{bmatrix} \mathbf{x}_m^\top | \boldsymbol{\eta}^\top \end{bmatrix}^\top \\ &= \begin{bmatrix} x & y & \cdots & \eta_1 & \eta_2 & \cdots \end{bmatrix}^\top \end{aligned} \tag{6}$$

where $\mathbf{x}_m$ is the vehicle state vector, and $\boldsymbol{\eta}$ is the elevation vector, where η_i is the elevation at the ith node.

State augmentation results in a state-parameter estimation problem associated with sensor measurements. The EKF algorithm is used in this study because the system and measurement equations involve nonlinearities, in which nonlinear equations are linearized through a numerical Jacobian for every step and adopted to the linear Kalman filter form. The EKF is a commonly-used SLAM filter algorithm due to its computational efficiency and well-established systematic design procedure. This study also uses the EKF filter algorithm.

In Kalman filtering, the uncertainty in the state estimate is represented using the error covariance matrix with the assumption that it follows a multivariate normal distribution. This error covariance matrix is associated with the augmented state vector in Eq. (6). Its dimensions are $(n_0+m)\times(n_0+m)$, where n_0 is the dimension of the vehicle's motion state vector and m is the dimension of the surface elevation vector (equal to the total number of nodal points). The matrix can be

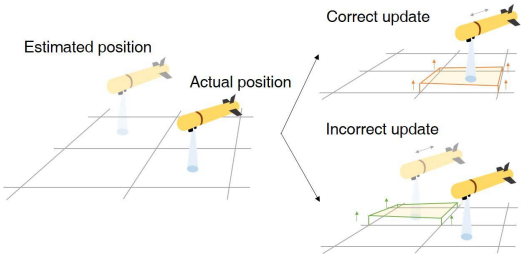

FIGURE 3. Example of incorrect update when the panels of the actual vehicle and estimated location differ.

partitioned as

$$\mathbf{P} = \left[\begin{array}{c|c} \mathbf{P}_{\mathbf{x}_m\mathbf{x}_m} & \mathbf{P}_{\mathbf{x}_m\eta} \\ \hline \mathbf{P}_{\eta\mathbf{x}_m} & \mathbf{P}_{\eta\eta} \end{array}\right]. \tag{7}$$

D. UPDATE IN EKF-SLAM FILTER

The topographic map representation enables the new SLAM approach combined with grid-basd SLAM and feature-based SLAM. The proposed map structure has a similar aspect with the grid-based map representation because it represents the height of the terrain at regular grid spacing. However, estimation of the terrain map state follows the feature-based SLAM approach. In the feature-based SLAM algorithm, data association of landmarks is a significant issue for loop-closure, achieved by matching the updating panel belonging to the actual vehicle. Naive implementation would assume that the estimator can sufficiently know the vehicle's position, and the updated panel is chosen based on where the estimated position of the vehicle belongs. However, invalid data assocation involves latent instability that can lead to filter divergence, as depicted in Fig. 3.

Dynamic grid adaptation (DGA) and WGP have been proposed based on the state probability distribution [27], [28] to address this data association. DGA determines the panel size to include the area of all confidence intervals of a vehicle's position so that the actual vehicle must be located in the updated panel. However, because the modeling error from the bilinear interpolation increases when the panel size increases, DGA should be used with a small grid-size setting, which is daunting for long-term operation. Therefore, WGP is adopted in this paper because of its superior applicability regardless of the panel grid size.

The WGP method does not determine the vehicle's panel but instead updates all the possible states based on the state probability distribution. The confidence interval, representing the possible regions where the vehicle is located, is inferred from the mean estimate and associated covariance; panels overlapping with the confidence interval are sorted out. State distribution is separated according to the selected grid using the pdf truncation method. Suppose that the probability distribution is truncated according to the grid located at (x_g, y_g) with grid size (dx, dy). The inequality constraints on the position vector are:

$$\begin{aligned} x_g \le x \le x_g + dx \\ y_g \le y \le y_g + dy. \end{aligned} \tag{8}$$

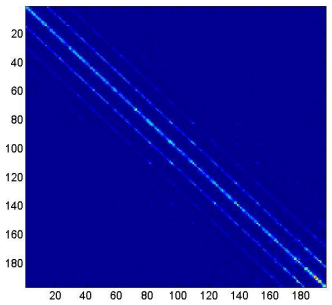

FIGURE 4. Visualization of the steady-state correlation between the surface elevation states in the map. The error covariance matrix $P_{\eta\eta}$ is visualized as an image plot.

Applying an inequality constraint requires several numerical techniques using Eigen decomposition and Gram-Schmidt orthogonalization. After the truncation, each distribution $\mathbf{x}^i$, $\mathbf{P}^i$ according to the grid belongs to a specific panel and is independent. Consequently, they can be updated without causing filter divergence.

E. SCALABILITY ISSUE

The dimensions of the elevation vector increase rapidly with the increase in the size of the map (or the map resolution), significantly increasing computational cost. This problem can be circumvented by adaptively configuring the system's state vector and the associated error covariance matrix for measurement updates.

Figure 4 illustrates the correlation in the error covariance matrix of the elevation vector, $P_{\eta\eta}$, at steady state. Several separated diagonal lines are observed in the plot. The matrix elements were linearly indexed, moving from one column to the next to transform the spatially distributed nodes into vectors. In Fig. 4, the diagonal line represents the self-correlation, and the off-diagonal lines suggest the periodic cross-correlation between the neighboring nodes, which states that the correlation effect of the selected node is confined to some finite number of surrounding nodes. Accordingly, it can be conjectured that the effect of measurement update is significant only for the nodal points close to the position where the measurement is taken.

State $\mathbf{x}_{\eta,a}$ is selected as the possible map state where the vehicle belongs, as depicted in Fig. 5. State $\mathbf{x}_{\eta,a}$ surrounding state $\mathbf{x}_{\eta,a}$ only correlates with $\mathbf{x}_{\eta,a}$, and state $\mathbf{x}_{\eta,c}$ surrounding state $\mathbf{x}_{\eta,b}$ correlates only with state $\mathbf{x}_{\eta,b}$ among the farther map states. As it continues to cover all the map states, the covariance matrix of the map state and Jacobian matrix H are represented as follows:

$$\mathbf{P}_{\eta\eta} = \left[\begin{array}{c|c|c|c} \mathbf{P}_{aa} & \mathbf{P}_{ab} & 0 & 0 \\ \hline \mathbf{P}_{ba} & \mathbf{P}_{bb} & \mathbf{P}_{bc} & 0 \\ \hline 0 & \mathbf{P}_{bc} & \mathbf{P}_{cc} & \dots \\ \hline 0 & 0 & \dots & \dots \end{array}\right] \tag{9}$$

$$H = \begin{bmatrix} H_a & 0 & 0 & \dots \end{bmatrix}^\top. \tag{10}$$

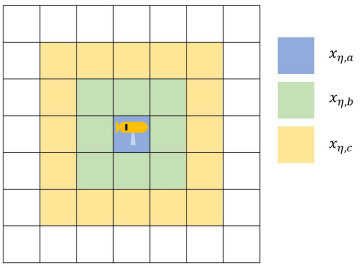

FIGURE 5. Visualization of the map state division according to correlation.

The Kalman gain K and the update term dP of the covariance matrix can be then be evaluated only using the related variables of states $\mathbf{x}_{\eta,a}$ and $\mathbf{x}_{\eta,b}$.

$$K = \begin{bmatrix} P_{aa}H_a^T/(H_aP_{aa}H_a^T + r) \\ P_{ba}H_a^T/(H_aP_{aa}H_a^T + r) \\ 0 \\ \cdots \end{bmatrix} \tag{11}$$

$$dP = KSK^T \tag{12}$$

This enables approximating the original full SLAM problem as a smaller problem involving a vector with reduced dimensions and associated error covariance, denoted as $\mathbf{x}^s$ and $\mathbf{P}^s$, respectively. The reduced state vector is augmented and represented as

$$\begin{aligned} \mathbf{x}^s &= \begin{bmatrix} \mathbf{x}_m^\top \end{bmatrix} \quad \boldsymbol{\eta}^{s\top} \end{bmatrix}^\top \\ &= \begin{bmatrix} \mathbf{x}_m^\top \end{bmatrix} \quad \eta_i \quad \eta_{i+1} \quad \cdots \quad \eta_j \quad \eta_{j+1} \quad \cdots \end{bmatrix}^\top \end{aligned} \tag{13}$$

where $\boldsymbol{\eta}^s$ is the reduced elevation vector whose nodal points are located around the estimated vehicle's position at which the current elevation measurement is provided. The reduced error covariance matrix, $\mathbf{P}^s$, is updated locally and registered back to the original global map. This update scheme closely resembles the submapping SLAM methods with partitioned updates [29], [30]. Because the dimensions of the reduced system are independent of the size of the mapping area, the computational cost for each iteration remains unchanged. This is advantageous in solving large-scale SLAM problems.

A smaller submap improves computational efficiency but may degrade the filter's performance, particularly in terms of stability when the correlation is not zero. Thus, the size of the submap must be carefully considered.

V. TOPOGRAPHIC SLAM SIMULATIONS

Simulations were conducted on a scenario where an AUV performs a bathymetric SLAM operation in the area of interest to verify the feasibility and validity of the proposed SLAM approach. Actual bathymetric data were used to create a realistic simulation environment.

A. VEHICLE DYNAMICS FOR SIMULATIONS

A simplified vehicle dynamics model is introduced based on practical considerations to demonstrate the SLAM capability. The altitude of the vehicle in the vertical plane is measured using a pressure transducer, and drift-free pitch and roll angle measurements are provided by tilt sensors. Given this sensing capability, it is assumed that the vertical position and the attitude in the heave, roll, and pitch modes are stabilized through closed-loop feedback control. Furthermore, the vehicle dynamics model with no side-slip is introduced by assuming that the vehicle's drift is minimal. These assumptions enable decoupling the inner-loop motion control from the vehicle navigation problem and reducing the state dimensions of the system dynamics model, simplifying this SLAM filter formulation. The resulting reduced state vector $\mathbf{x}$ for describing the simplified vehicle's motion in the horizontal plane is obtained as

$$\mathbf{x}_m = \begin{bmatrix} x & y & \psi & V \end{bmatrix}^\top \tag{14}$$

where x, y, and ψ are the position and heading coordinates, and V is the longitudinal velocity. The system dynamics can be expressed in the state-space form as

$$\dot{\mathbf{x}}_m = \mathbf{f}_m(\mathbf{x}_m, \mathbf{u}, \mathbf{w}) = \begin{bmatrix} V\cos\psi \\ V\sin\psi \\ u_1 \\ u_2 \end{bmatrix} + \mathbf{w} \tag{15}$$

where $\mathbf{w}$ is the process noise. The control input vector is defined as $\mathbf{u} = [u_1 \quad u_2]^\top$, in which u_1 is the heading rate control input and u_2 is the longitudinal acceleration control input.

Moreover, the measurement vector $\mathbf{z}$ is composed of the yaw angle, longitudinal velocity, and vertical distance measurement to the terrain surface from the vehicle.

$$\mathbf{z} = \mathbf{h}(\mathbf{x}_m, \eta, \mathbf{v}) = \begin{bmatrix} \psi \\ V \\ \eta \end{bmatrix} + \mathbf{v} \tag{16}$$

where the $\mathbf{v}$ is the measurement noise. In the water, the velocity V is often measured using a speed sensing device such as a DVL or pitot tube. The yaw angle ψ can be provided by a compass or a gyro.

B. TERRAIN DATA AND SIMULATION SETTINGS

Actual bathymetric data near the coast of Taean in the West Sea of Korea (Yellow Sea) (Fig. 6) were used for the simulation study. The bathymetric data were obtained through surveys using a high-resolution MBE mounted on a surface vessel and then post-processed. The resulting bathymetric map is depicted in Fig. 7.

A vehicle was assumed to carry a terrain altimeter, which provides range measurements between the vehicle and the terrain surface. Initially, the terrain elevations were assumed to be unknown, and the elevations of the nodal points were set as altitude measurement values. Both the water depths at these nodal points and the vehicle's position were estimated simultaneously using a sequence of depth measurements provided by the single altimeter sensor. The grid dimension for reconstructing the terrain map based on the topographic SLAM was set to be much lower than

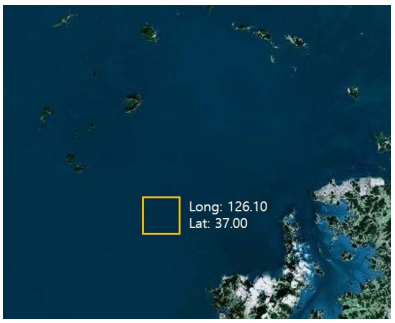

FIGURE 6. Survey site off the coast of Taean in the West Sea of Korea (Yellow Sea).

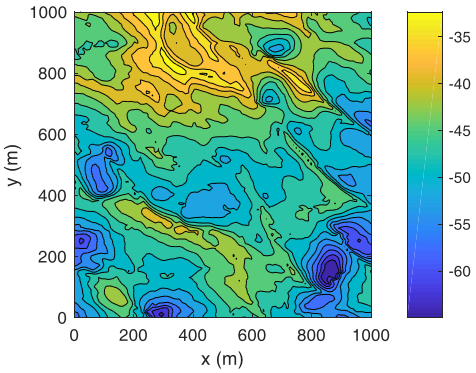

FIGURE 7. Contour plots of digital elevation model (DEM) of the actual bathymetry of the survey site.

TABLE 1. Parameter settings of the SLAM filter.

Parameters	Values
Mapping area	100×300 (m)
Grid coordinate dimension (T-SALM)	10×30
Nominal vehicle speed, V	5 (knots)
Sampling rate (motion sensors)	10 (Hz)
Sampling rate (terrain altimeter)	1 (Hz)
Process noise in heading (1σ)	2°
Process noise in speed (1σ)	0.02 (m/sec)
Measurement noise in heading (1σ)	2°
Measurement noise in speed (1σ)	0.02 (m/sec)
Measurement noise in altitude (1σ)	1.0 (m)

that of the original to reduce computational requirements by approximating the continuous terrain surface as a set of rectangular patches stitched together. A grid dimension of 30 by 10 (grid size = 10 m) was used for the SLAM operation. The parameter settings for the simulations are presented in Table 1. Tidal effects were not considered in this study.

This study assumes that the distance from the vehicle to the terrain surface is measurable and the depth from the water surface is maintained as constant via feedback control. In the horizontal direction, the vehicle follows a lawnmower pattern with 10-m widths between the paths. Once the vehicle finishes the one lawnmower pattern trajectory, it returns to the starting point and follows a lawnmower pattern in the other direction. At least four altitude measurements are required in one panel to estimate the elevations of nodal points, and the places where the measurements are obtained should differ.

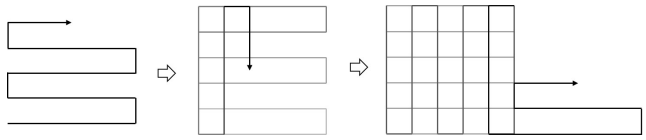

FIGURE 8. Vehicle trajectory following the repeated lawnmower pattern. After fully estimating the covered map, the vehicle starts a new lawnmower pattern trajectory.

If the measurements are obtained in one direction, it is possible to have multiple solutions for determining elevations of nodal points, although the number of obtained measurements is over four. Therefore, the topographic map should be estimated precisely by revisiting the area from the other direction. The length of one lawnmower pattern depends on the motion sensor's ability not to lose the position until complete. Once the bathymetric map is fully estimated, the SLAM algorithm operates as TRN with a known map. After fully estimating the map, the vehicle moves to the undiscovered area to survey. This moving pattern is adequate for surveillance and reconnaissance in real-world applications. Fig. 8 illustrates the vehicle trajectory in consecutive order.

Various simulations are designed to discuss the characteristics of the proposed topographic SLAM. First, the performance is compared to dead-reckoning. We performed SLAM according to various regions in the given bathymetric map because each region has different altitude variations. The predicted localization accuracy increases with the altitude variation, but not significantly. The simulations were performed 100 times in the same environment because the process noise and measurement noise are randomly generated, resulting in different SLAM results each time. The physical time duration of the simulation was set as 2,500 seconds.

Second, the vehicle is set to move in the region for a long time after estimating the terrain to verify whether the position estimate is bounded. The vehicle moves for 5,000 seconds more establishing the map.

Finally, mapping accuracy according to the grid size is investigated because it is crucial to compensate between mapping accuracy and computation. Moreover, it is not always suitable to have a small panel grid size because it requires many more measurements to estimate the map variables.

C. ESTIMATED TRAJECTORY THROUGH SLAM

To the best of the authors' knowledge, there has been no attempt in topographic SLAM using a single beam acoustic altimeter, and the performance of the proposed algorithm is demonstrated through the comparison with the performance by dead-reckoning. In the dead-reckoning simulation, no altitude measurement relative to the terrain surface was provided to the navigation filter system, and drift

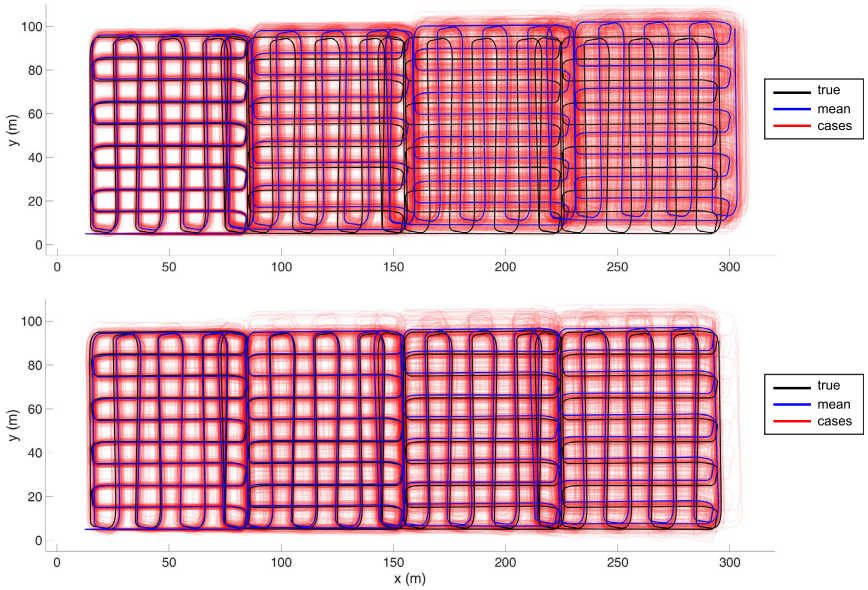

FIGURE 9. Estimated vehicle trajectories of 100 Monte-Carlo simulations by dead-reckoning (top) and topographic SLAM (bottom). The estimated dead-reckoning trajectory of the vehicle was considerably shifted away from the desired trajectory due to drift errors. The error in the trajectory estimate by topographic SLAM was significantly reduced in comparison with the case of dead-reckoning.

error would accumulate. The drift error was intentionally exaggerated in this simulation to evaluate the proposed method by adding a slight bias to the velocity measurement. The distinct trajectory discrepancy between the actual and estimated values by dead-reckoning is depicted in Fig. 9.

In contrast, the position accuracy was significantly improved in the case of using topographic SLAM. Most of the estimated trajectories are closely consistent with the actual trajectory, and only several cases deviate slightly from the actual one. The proposed algorithm cannot always ensure accurate position estimation because dynamics models have inherent uncertainty; it must estimate the whole area within a finite amount of noise-mixed measurements. Nonetheless, the position error is not larger than dead-reckoning even for the worst-case trajectory when using a topographic SLAM.

Remarkably, the position estimate in the x-direction is more accurate than in the y-direction because the vehicle initially follows the lawnmower pattern of the x-direction. Before completing the map estimation, the update of the position is not sufficiently valid, and the error and uncertainty of the target position would increase. Consequently, the region of the upper area in the y-direction must be estimated with higher uncertainty in the vehicle's position, which produces more error.

D. LONG-TIME OPERATION

Fig. 10 illustrates the result when the vehicle follows the same trajectory but repeats the paths after finishing the one trajectory. In the previous scenario, the vehicle moves to next region to survey the undiscovered area as soon as all the visited areas are fully covered, causing a consistently

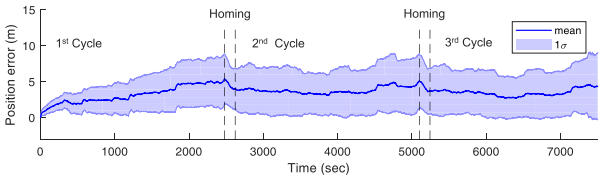

FIGURE 10. Average position error of 100 Monte-Carlo simulations according to time by dead-reckoning and topographic SLAM. The error graph illustrates distinctions between the terrain areas.

increasing error, although it is reduced compared with dead-reckoning. If the vehicle moves within the boundary after the map uncertainty converged, it performs similarly to a map-based TRN. Even the cases that the estimated trajectory has a discrepancy with the actual one, the estimated position of the vehicle is bounded in the map area established at the beginning. This implies that the topographic SLAM algorithm may not assure the exact position estimation, especially when discovering new regions, but it can prevent accumulation of drift error within the map once it is fully estimated.

The error confinement derives from the loop closure, returning to a previously visited area. In the general feature-based SLAM algorithm, the position estimate can converge close to the true position by loop closure because detecting known landmarks can directly inform the vehicle's global position. However, this does not occur with the proposed algorithm because the measurement of a single altimeter cannot be matched to a specific terrain area.

Instead, if we know that measurement comes from the area of specific panels and the elevations of nodal points

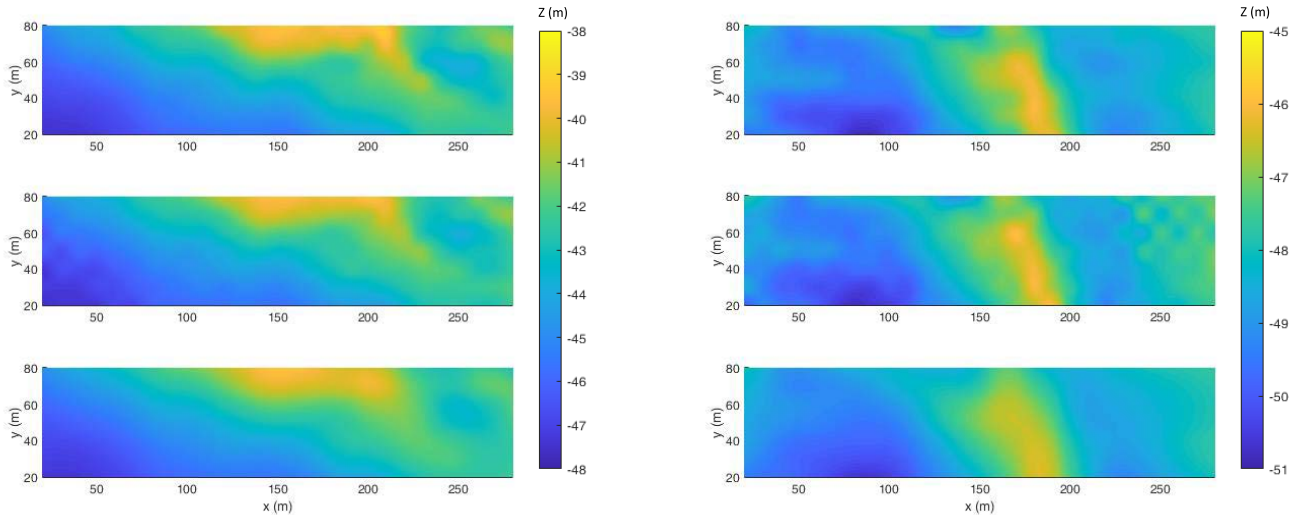

FIGURE 11. The topographic map (DEM) reconstructed by the SLAM filter with high-resolution and low-resolution settings. (From the top, ground truth bathymetry, reconstructed bathymetry using 10-m grid size, and reconstructed bathymetry using 20-m grid size.)

approximating the terrain surface, the position estimate is updated smoothly following the inclination of the corresponding panels. This smooth update also benefits from its robustness because it does not require exact data association or distinguishable terrain landmarks as does feature-based SLAM. Therefore, the surprising position update might not happen in the topographic SLAM, but it still results in suitable, stable estimation performance within the map boundary.

E. CHANGES IN THE MAP RESOLUTION

The resolution (i.e., grid size) of the topographic map is a crucial filter parameter that may significantly influence the performance of the topographic SLAM operation. Additional simulations with two unique grid resolution settings were performed: grid size $=$ 10 m and grid size $=$ 20 m. The resulting contour plots are depicted in Fig. 11.

In both cases, the physical mapping time was set identical to the previous case at 2,500 seconds. However, the computational complexity increases with the map resolution due to the increases in the filter's state dimensions. The computation time increases approximately quadratically with the grid resolution.

A higher map resolution setting will produce a more refined, detailed map. However, a higher resolution is not guaranteed to improve SLAM navigation and mapping performance, especially when the same amount of physical survey time is given with the same survey trajectory. This is because the map with a higher resolution involves more unknowns to be estimated, requiring more effort for the filter to estimate the increased number of states. Therefore, in addition to more extensive computation for each measurement update cycle, more survey time is required to achieve satisfactory mapping performance in a high-resolution setting.

VI. CONCLUSION

In this study, an EKF-based SLAM approach using topographic information was formulated and implemented. The simulation results demonstrate the feasibility and utility of the proposed topographic SLAM approach.

Although the MBE is a more commonly-used and effective topographic sensor for seabed terrain mapping, it cannot be easily integrated into a lost-cost small AUV due to its weight, power consumption, and computational cost. Therefore, this study focused on developing a computationally efficient algorithm for navigation and map-building operations using a single-beam acoustic altimeter on a small vehicle platform with limited sensing and computational capabilities.

Accordingly, the topographic SLAM method was newly formulated and applied, which greatly simplifies the map representation for the topographic SLAM by parameterizing any given undulating terrain surface using a number of rectangular panels. The nodal points of those panels were introduced into the filter's state vector and estimated in the EKF framework. Based on the estimated probability, the WGP was used for data association of updating the panel, and the algorithm's scalability issue was addressed.

The simulation study was performed using actual subsea terrain data, and its results were discussed. The SLAM results with different terrain variations, long operation times, and different map resolution settings were discussed. This study demonstrated the potential benefits of the proposed algorithm in terms of both navigation and map-building.

ACKNOWLEDGMENT

The authors would like to thank to Dr. Yosup Park with the Korea Institute of Ocean Science and Technology, for providing the high-resolution bathymetric data.

REFERENCES

[1] W. Baker and R. Clem, "Terrain contour matching [TERCOM] primer," Aeronaut. Syst. Division, Wright-Patterson AFB, Wright-Patterson AFB, OH, USA, Tech. Rep. TR-77-61, 1977.

[2] L. Hostetler, "Optimal terrain-aided navigation systems," in *Proc. AIAA Guid. Control Conf.*, Aug. 1978, doi: 10.2514/6.1978-1243.

[3] M. Cowie, N. Wilkinson, and R. Powlesland, "Latest development of the TERPROM digital terrain system (DTS)," in *Proc. IEEE/ION Position, Location Navigat. Symp.*, May 2008, pp. 1219–1229.

[4] A. E. Johnson and J. F. Montgomery, "Overview of terrain relative navigation approaches for precise lunar landing," in *Proc. IEEE Aerosp. Conf.*, Mar. 2008, pp. 1–10.

[5] M. Sistiaga, J. Opderbecke, M. Aldon, and V. Rigaud, "Map based underwater navigation using a multibeam echosounder," in *Proc. IEEE Ocean. Eng. Soc. (OCEANS)*, vol. 2, Sep./Oct. 1998, pp. 747–751.

[6] I. Nygren and M. Jansson, "Terrain navigation for underwater vehicles using the correlator method," *IEEE J. Ocean. Eng.*, vol. 29, no. 3, pp. 906–915, Jul. 2004.

[7] D. K. Meduna, S. M. Rock, and R. McEwen, "Low-cost terrain relative navigation for long-range AUVs," in *Proc. OCEANS*, 2008, pp. 1–7.

[8] C. Morice, S. Veres, and S. McPhail, "Terrain referencing for autonomous navigation of underwater vehicles," in *Proc. OCEANS-EUROPE*, May 2009, pp. 1–7.

[9] G. Salavasidis, A. Munafò, and D. Fenucci, "Terrain-aided navigation for long-range AUVs in dynamic under-mapped environments," *J. Field Robot.*, vol. 38, no. 3, pp. 402–428, 2021.

[10] S. Carreno, P. Wilson, P. Ridao, and Y. Petillot, "A survey on terrain based navigation for AUVs," in *Proc. OCEANS MTS/IEEE SEATTLE*, Sep. 2010, pp. 1–7.

[11] R. C. Smith and P. Cheeseman, "On the representation and estimation of spatial uncertainty," *Int. J. Robot. Res.*, vol. 5, no. 4, pp. 56–68, 1986.

[12] J. Leonard and H. Durrant-Whyte, "Simultaneous map building and localization for an autonomous mobile robot," in *Proc. Intell. Robots Syst. Intell. Mech. Syst. IEEE/RSJ Int. Workshop (IROS)*, vol. 3, Nov. 1991, pp. 1442–1447.

[13] S. Thrun, W. Burgard, and D. Fox, *Probabilistic Robotics*. Cambridge, MA, USA: MIT Press, 2005.

[14] J. Kim and S. Sukkarieh, "Autonomous airborne navigation in unknown terrain environments," *IEEE Trans. Aerosp. Electron. Syst.*, vol. 40, no. 3, pp. 1031–1045, Jul. 2004.

[15] J. Langelaan and S. Rock, "Towards autonomous UAV flight in forests," in *Proc. AIAA Guid., Navigat., Control Conf. Exhibit*, San Francisco, CA, USA, Aug. 2005, p. 5870.

[16] A. Paul and E. Wan, "Dual Kalman filters for autonomous terrain aided navigation in unknown environments," in *Proc. IEEE Int. Joint Conf. Neural Netw.*, vol. 5, Jul./Aug. 2005, pp. 2784–2789.

[17] C. Roman and H. Singh, "Improved vehicle based multibeam bathymetry using sub-maps and SLAM," in *Proc. IEEE/RSJ Int. Conf. Intell. Robots Syst.*, Aug. 2005, pp. 3662–3669.

[18] T. Maki, H. Kondo, T. Ura, and T. Sakamaki, "Imaging vent fields: SLAM based navigation scheme for an AUV toward large-area seafloor imaging," in *Proc. IEEE/OES Auto. Underwater Vehicles*, Oct. 2008, pp. 1–10.

[19] P. Norgren and R. Skjetne, "A multibeam-based SLAM algorithm for iceberg mapping using AUVs," *IEEE Access*, vol. 6, pp. 26318–26337, 2018.

[20] S. Barkby, S. B. Williams, O. Pizarro, and M. V. Jakuba, "A featureless approach to efficient bathymetric SLAM using distributed particle mapping," *J. Field Robot.*, vol. 28, no. 1, pp. 19–39, Jan. 2011, doi: 10.1002/rob.20382.

[21] S. Barkby, S. B. Williams, O. Pizarro, and M. V. Jakuba, "Bathymetric particle filter SLAM using trajectory maps," *Int. J. Robot. Res.*, vol. 31, no. 12, pp. 1409–1430, Oct. 2012.

[22] A. Palomer, P. Ridao, and D. Ribas, "Multibeam 3D underwater SLAM with probabilistic registration," *Sensors*, vol. 16, no. 4, p. 560, Apr. 2016.

[23] T. Ma, Y. Li, R. Wang, Z. Cong, and Y. Gong, "AUV robust bathymetric simultaneous localization and mapping," *Ocean Eng.*, vol. 166, pp. 336–349, Oct. 2018.

[24] R. A. Stuckey, "Navigational error reduction of underwater vehicles with selective bathymetric SLAM," *IFAC Proc. Volumes*, vol. 45, no. 5, pp. 118–125, 2012.

[25] V. Bichucher, J. M. Walls, P. Ozog, K. A. Skinner, and R. M. Eustice, "Bathymetric factor graph SLAM with sparse point cloud alignment," in *Proc. OCEANS–MTS/IEEE Washington*, Oct. 2015, pp. 1–7.

[26] S.-H. Mok and H. Bang, "Terrain slope estimation methods using the least squares approach for terrain referenced navigation," *Int. J. Aeronaut. Space Sci.*, vol. 14, no. 1, pp. 85–90, Mar. 2013.

[27] J. Jang and J. Kim, "Dynamic grid adaptation for panel-based bathymetric SLAM," in *Proc. IEEE Underwater Technol. (UT)*, Apr. 2019, pp. 1–4.

[28] J. Jang and J. Kim, "Weighted grid partitioning for panel-based bathymetric SLAM," in *Proc. OCEANS–Marseille*, Jun. 2019, pp. 1–6.

[29] J. E. Guivant and E. M. Nebot, "Optimization of the simultaneous localization and map-building algorithm for real-time implementation," *IEEE Trans. Robot. Autom.*, vol. 17, no. 3, pp. 242–257, Jun. 2001.

[30] T. Bailey and H. Durrant-Whyte, "Simultaneous localization and mapping (SLAM): Part II," *IEEE Robot. Autom. Mag.*, vol. 13, no. 3, pp. 108–117, Sep. 2006.

JUNWOO JANG received the B.S. degree in mechanical engineering from the Korea Advanced Institute of Science and Technology (KAIST), Daejeon, South Korea, in 2017, where he is currently pursuing the integrated M.S. and Ph.D. degree with the Department of Mechanical Engineering.

His research interests include underwater navigation and reinforcement learning for maritime systems.

JINWHAN KIM (Member, IEEE) received the B.S. and M.S. degrees in naval architecture and ocean engineering from Seoul National University, Seoul, South Korea, and the Ph.D. degree in aeronautics and astronautics from Stanford University. He is currently with the Faculty of Mechanical Engineering, Korea Advanced Institute of Science and Technology, Daejeon, South Korea. He is a Senior Member of AIAA.